Sensorless Tilt Compensation for a Three-Axis Optical Pickup Using a Sliding-Mode Controller Equipped With a Sliding-Mode Observer

Paul C.-P. Chao and Chien-Yu Shen

***Abstract*—A sliding-mode controller equipped with a sliding-mode observer is synthesized and applied to a novel three-axis four-wire optical pickup for the purpose of sensorless tilt compensation. The three-axis pickup owns the capability to move the lens holder in three directions of focusing, tracking and tilting, which is required particularly for higher data-density optical disks and precision measuring instruments to annihilate nonzero lens tiltings. To achieve the sensorless compensation, Lagrange's equations are first employed to derive equations of motion for the lens holder. A sliding-mode controller is then designed to perform dynamic decoupling and forge control efforts toward the goals of precision tracking, focusing, and zero tilting. Along with the controller, a sliding-mode observer is designed to perform the online tilt estimation of the lens holder. This estimated tilt allows the previously designed sliding-mode controller to be implemented in most existing commercial pickups without additional photodiodes to detect the tilting motion of the lens holder. A full-order high-gain observer is next forged to estimate the moving velocities of the lens holder in order to provide low-noised feedback velocity signals for the designed sliding-mode controller. Simulations are carried out to choose appropriate controller and observer gains. Finally, experiments are conducted to validate the effectiveness of the controller for annihilating lens tilting and the capability of the tilt observer for performing sensorless tilt compensation.**

***Index Terms*—High-gain observer, sensorless compensation, sliding-mode controller, sliding-mode observer, three-axis optical pickup.**

I. Introduction

FOR OPTICAL disk drives (ODDs) and some surface-profiling instruments in micro- or nano-precision [1]–[3], the key component determining the performance is the optical pickup, which conducts data-reading via a well-designed optical system installed inside the pickup. Fig. 1 shows a photograph of a three-axis four-wire-type pickup actuator, which is designed and manufactured by the Industrial Technology and Research Institute (ITRI) of Taiwan. This pickup consists mainly of an objective lens, a lens holder (often called "bobbin"), wire springs, sets of wound coils, and permanent magnets. Thanks to the flexibility of the wire springs, the bobbin could easily be in motion as the forces acting on the bobbin are generated by the electromagnetic interactions between the magnetic fields induced by permanent magnets and the currents conducted in sets of coils. A conventional pickup actuator (not the three-axis one shown in Fig. 1) often owns only two sets of wound coils—the focusing and tracking coils and the associated magnets. In this way, two independent actuating forces are generated in the directions of focusing (vertical to the disk) and tracking (horizontal to the disk) to perform precision positioning of the lens. This type of actuator is commonly named a "two-axis actuator."

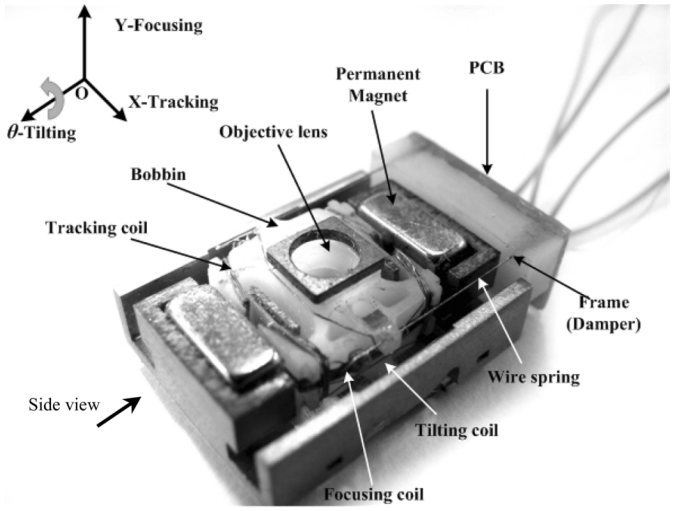

Fig. 1. Structure of the three-axis four-wire-type optical pickup by ITRI.

High numerical apertures (NAs) and short-wavelength laser diodes (like violet diodes) have recently been employed for objective lens designs in pickups in order to produce a smaller optical detecting spot on an optical disk for better data-reading resolution. This aims at increasing detectable data density via decreasing the circular radius of the aberration region of the optical spot, which is the main factor limiting resolution of data storage in disks for ODDs or surface profiling for measuring instruments. With the size of the optical spot decreased, original electromechanical designs of the pickup structure might become obsolete. One of the critical challenges arises from the unavoidable tilting of the bobbin during its motion since the resulted coma aberration increases in proportion to NA^3/λ, where λ is

Manuscript received September 03, 2006; revised November 04, 2007. Manuscript received in final form April 03, 2008. First published June 13, 2008; current version published February 25, 2009. Recommended by Associate Editor S. Devasia. This work was supported in part by the National Science Council of ROC through Contract 96-2221-E-009-069 and Contract 96-2622-E-009-010-CC3 and by the NCTU "Building Foundation" Project.

P. C.-P. Chao is with the Department of Electrical and Control Engineering National Chiao Tung University, Hsinchu 300, Taiwan, R.O.C. (e-mail: pchao@mail.nctu.edu.tw).

C.-Y. Shen is with the Department of Mechanical Engineering Chung-Yuan Christian University, Chung-Li 32023, Taiwan, R.O.C. (e-mail: jackalshen@gmail.com).

Digital Object Identifier 10.1109/TCST.2008.924560

the wavelength of the laser diode [4]. This tilting arises from two possible factors. The first factor is an uneven magnetic field due to manufacturing tolerance and/or the mispass of the net electromagnetic force in the directions of focusing and tracking to the mass center of the bobbin while the bobbin moves from its static position to desired vertical and radial positions. This factor leads to a tilting moment on the bobbin and then a nonzero bobbin tilt. The second factor is the unavoidable small unparallelism in practice between the lens and the optical disc in high-speed rotations or the surface to profile. To restrain the bobbin tilting to a small level for more accurate, faster data-reading, some research works [5]–[10] have successfully developed the tilt servo systems for the bobbin, in addition to original focusing and tacking ones. The tilt servo makes possible the capability of suppressing the unavoidable bobbin tiltings. The new pickups with tilt servo are often called the "three-axis" optical pickups. Fig. 1 shows one that was designed and fabricated by ITRI.

Among the aforementioned studies [5]–[10], Chao *et al.* [9], [11], [12] had established the equations governing the dynamics of the bobbin and designed a robust sliding-mode and intelligent controllers and a high-gain observer that is able to perform simultaneous positionings in three degrees of freedom (DOFs) of tracking, focusing, and tilting. The sliding-mode controller (SMC) [13], [14] was chosen due to its advantages (when compared with well-known H^{∞} controllers) of the robustness against parameter uncertainties and the capability to tackle system couplings and nonlinearities. However, the SMC in practice needs to acquire online feedbacks of bobbin motions not only in DOFs of focusing and tracking but also tilting. For conventional pickups, only motions of tracking and focusing can be detected by specifically designed optical systems and several patches of photo-detectors [15]. Fig. 2 illustrates a typical optical/sensing system for measuring the motions of the bobbin, where Fig. 2(a) illustrates the overall optical system, Fig. 2(b) shows the basic principle of quad-detectors for detecting focusing motions, and Fig. 2(c) demonstrates the three-beam method for tracking motions. It is can easily be seen from Fig. 2 that the conventional optical system needs additional patches of photo-detectors or apply the recently proposed methods of signal analysis [16]–[18] on the reflected light intensity to equip itself with the capability of tilt detection. The former approach requires significant hardware modification, while the latter arrives reportedly at moderate accuracies due to sensor sensitivity variation and/or geometry of the disk surface. To circumvent the aforementioned shortcomings, a sliding-mode observer [19]–[26] is synthesized in this study to perform the online estimation of the tilting motions of the bobbin based on the motions in focusing and tracking detected by the original commercial optical systems, as shown in Fig. 2. The estimated tilting motion allows the predesigned SMC to be implemented in all existing commercial pickups without any hardware modification on the conventional optical disk drives. Along with the sliding-mode controller and observer is a full-order high-gain observer [27]–[33] forged in this study to estimate bobbin velocities in practice, which is aimed to provide low-noise feedback velocity signals for the designed SMC. Experiments are finally conducted to verify the effectiveness of the designed SMC scheme for annihilating bobbin tilting and

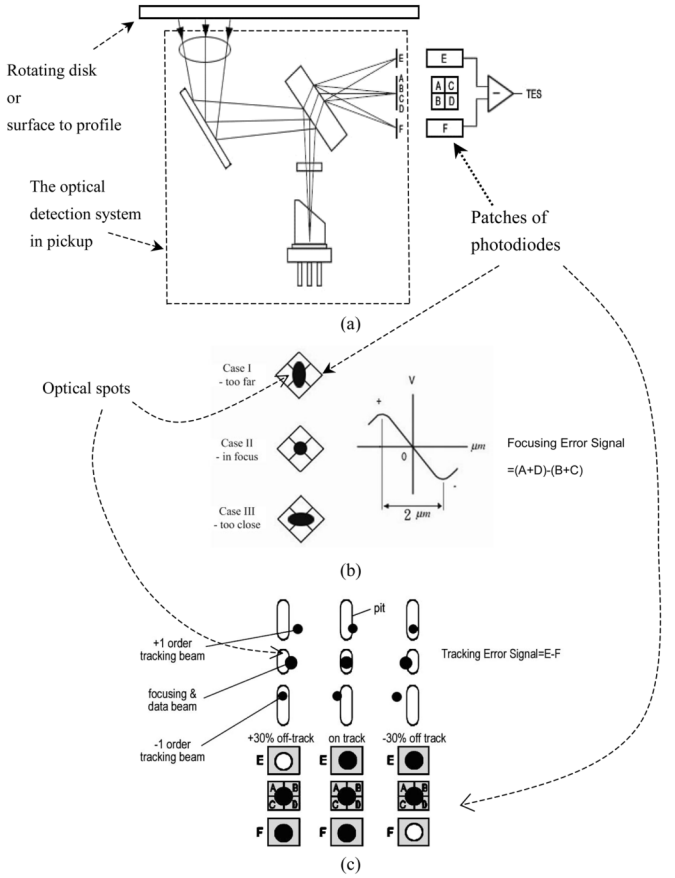

Fig. 2. (a) Optical system of the pickup including photodiodes. (b) Method of quad-detectors measuring focusing error. (c) Three-beam method for measuring tracking error [15].

the capability of the observers for estimating the bobbin tilting motions and reducing the effects of digital noise while pickup in positioning.

This paper is organized as follows. Section II presents the mathematical modeling of the three-axis four-wire-type lens actuator. Section III presents the design of the SMC and the high-gain observer, while Section IV offers the synthesis of the sliding-mode tilt observer. The numerical and experimental results are presented in Sections V and VI, respectively, to predict and verify the performance of the proposed controller/observer scheme. Finally, conclusions are given in Section VII.

II. Mathematical Modeling

A. Dynamic Modeling of the Bobbin

A typical three-axis pickup actuator designed and fabricated by ITRI as shown in Fig. 1 is considered in this study. The conventional bobbin, due to its specially designed supporting structure of four parallel wires, exhibits motions mainly in the DOFs of tracking $(X\text{-axis})$ and focusing $(Y\text{-axis})$. In addition to the motions in the X- and Y-directions, small tilting often occurs about the θ-axis, which is caused by manufacturing tolerance, uneven magnetic fields, and/or geometric mis-passes of the electro-magnetic forces acting line on the bobbin mass center. It is assumed that the pickup assembly can be simply modeled as a lumped mass-spring-damper system due to

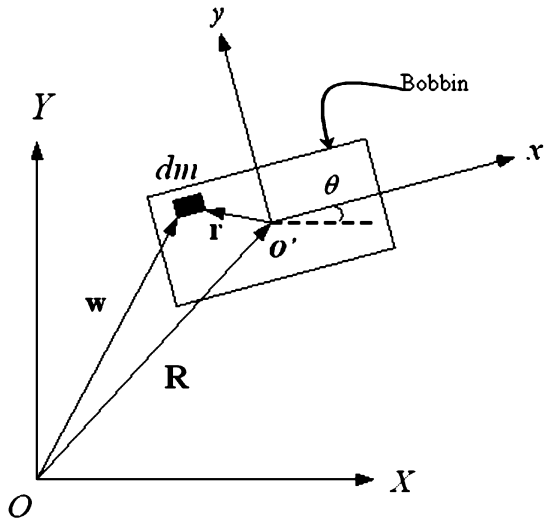

Fig. 3. Planar dynamic model of the bobbin from the side view in Fig. 1.

bobbin's high material rigidity compared with the flexibility of the suspending wires. Fig. 3 shows the schematic on the bobbin from the planar side view of Fig. 1 (from the viewpoint toward the X–Y plane) and accompanying coordinates/notations defined for capturing the bobbin motion. Shown in Figs. 1 and 3 are coordinates xyz defined as the body-fixed ones to the moving bobbin, while coordinates XYZ are global ground coordinates. X also serves as a dynamic variable, capturing the horizontal, tracking motion; Y does the vertical focusing motion; θ does the rotating angle of the bobbin about Z, i.e., the tilting angle. The displacement vector $\mathbf{w}$ for a given point of the bobbin can be captured by

$$\mathbf{w} = \mathbf{R} + \mathbf{Tr} \tag{1}$$

where $\mathbf{R} = [X \quad Y \quad 0]^T$ is the position vector of bobbin centroid O, measured from the origin of the ground coordinates XYZ, O. Also

$$\mathbf{T} = \begin{bmatrix} \cos\theta & -\sin\theta & 0 \\ \sin\theta & \cos\theta & 0 \\ 0 & 0 & 1 \end{bmatrix}$$

is the transformation matrix due to θ and $\mathbf{r} = [x \quad y \quad \theta]$ is the position vector of a differential mass (dm) in the bobbin, as shown in Fig. 3. Differentiating (1) with respect to time and putting into kinetic energy, the kinetic energy of the bobbin can be obtained as

$$\begin{aligned} L_T &= \frac{1}{2}\int_m \dot{\mathbf{w}}^T\dot{\mathbf{w}}\,\mathrm{dm} \\ &= \frac{1}{2}m(\dot{X}^2+\dot{Y}^2) + \frac{1}{2}I_\theta\dot{\theta}^2 \\ &\quad - \dot{X}\dot{\theta}(I_x\sin\theta + I_y\cos\theta) \\ &\quad + \dot{Y}\dot{\theta}(I_x\cos\theta - I_y\sin) \end{aligned} \tag{2}$$

where I_θ is the mass moment of inertia of the bobbin about its centroid along the z-axis, while $I_x = \int_m x\,\mathrm{dm}$ and $I_y = \int_m y\,\mathrm{dm}$ are first mass moments of inertia with respect to the x- and y-axes, respectively. The potential energy of the pickup is next expressed as

$$V = \frac{1}{2}(k_xX^2 + k_yY^2 + k_\theta\theta^2) + mgY \tag{3}$$

where k_x, k_y and k_θ are the equivalent spring stiffnesses in tracking, focusing, and tilting directions, m is the mass of bobbin, and g is the gravitation. Finally, the nonconservative virtual work can be derived as

$$\begin{aligned} \delta W &= \int_A (\mathbf{T}\cdot\mathbf{F})^T\delta\mathbf{w}\,\mathrm{dA} \\ &= (F_x\cos\theta - F_y\sin\theta)\delta X \\ &\quad + (F_x\sin\theta + F_y\cos\theta)\delta Y + F_\theta\delta\theta \end{aligned} \tag{4}$$

where δW denotes virtual work while F_x and F_y represent the actuation forces acting on the centroid, respectively, in the tracking and focusing directions. F_θ denotes the torsional moment about θ, and $\delta\mathbf{w}$ is the virtual bobbin displacement due to the applied force $\mathbf{F}$. Substituting (2)–(4) into Lagrange's equation [34], the equations of motion can be readily obtained as

$$\mathbf{M}\ddot{\mathbf{q}} + \mathbf{K}\mathbf{q} + \mathbf{N} + \mathbf{G} = \mathbf{TF} \tag{5}$$

where $\mathbf{q} = [X \quad Y \quad \theta]^T$ contains the generalized coordinates for describing the motion of the bobbin, $\mathbf{M}$ and $\mathbf{K}$ are overall mass and stiffness matrices, $\mathbf{N}$ contains the centrifugal and Coriolis force terms, $\mathbf{G}$ captures the gravitational effect, and $\mathbf{F}$ captures the actuator forces. Their expressions are given here, with $\mathbf{M}$ defined at the bottom of the page:

$$\mathbf{K} = \mathbf{diag}[k_x,\ k_y,\ k_\theta]$$

$$\mathbf{F} = [F_X \quad F_Y \quad F_\theta]^T$$

$$\mathbf{G} = [0 \quad mg \quad 0]^T$$

$$\mathbf{N} = \begin{bmatrix} -\dot{\theta}^2(I_x\cos\theta - I_y\sin\theta) \\ -\dot{\theta}^2(I_x\sin\theta + I_y\cos\theta) \\ \dot{X}\dot{\theta}(I_x\cos\theta - I_y\sin\theta) + \dot{Y}\dot{\theta}(I_x\sin\theta + I_y\cos\theta) \end{bmatrix}.$$

$$\mathbf{M} = \begin{bmatrix} m & 0 & -(I_x\sin\theta + I_y\cos\theta) \\ 0 & m & (I_x\cos\theta - I_y\sin\theta) \\ -(I_x\sin\theta + I_y\cos\theta) & (I_x\cos\theta - I_y\sin\theta) & I_\theta \end{bmatrix}$$

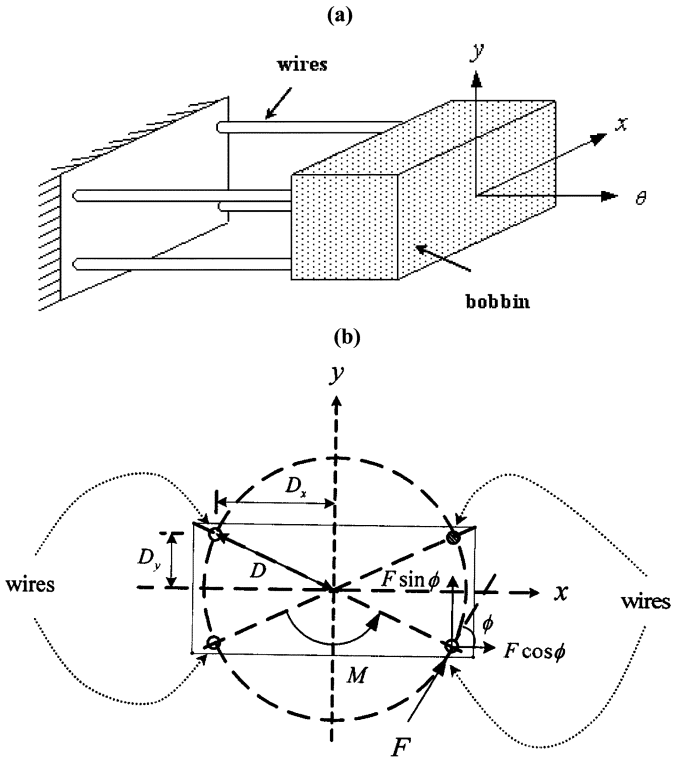

Fig. 4. Moment generation of the four-wire-type optical pickup. (a) 3-D view. (b) Side view of the bobbin from the positive direction.

The stiffness coefficients in the above $\mathbf{K}(k_x, k_y)$ comply with

$$k_x = k_y = 4 \cdot \frac{12EI_w}{L^3} \tag{6}$$

where E is the elastic modulus, I_w is the area moment of inertia about the x- or y-axis for the wire, and L is the length of each wire. The expression of k_θ is next due to be derived. To this end, Fig. 4 illustrates how to derive the moment M responsible for the tilting of the bobbin. In Fig. 4(b), F represents the combined electromagnetic force in focusing and tracking directions, which is generated by the current carried by a wire at some instant. ϕ is the angle between F and the x-axis. Assuming an even magnetic field, the electromagnetic forces induced by other three wires are identical and can also then be denoted by F. Then, the net moment acting on the bobbin is

$$M = 4FD$$

where D, as shown in Fig. 4(b), is the distance between the bobbin center and the wire. The angular deflection θ is next derived for calculating the equivalent rotational (tilting) stiffness k_θ, which is started with expressing the translational deflections in x and y directions due to the total electromagnetic force F as

$$\begin{aligned} \delta_x &= \frac{4F\cos\phi}{k_x} = \frac{F\cos\phi L^3}{12EI_w} \\ \delta_y &= \frac{4F\sin\phi}{k_y} = \frac{F\sin\phi L^3}{12EI_w}. \end{aligned} \tag{7}$$

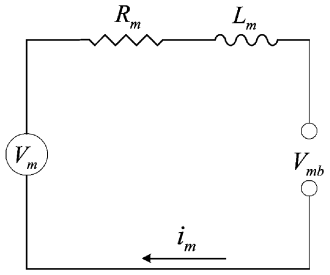

Fig. 5. Circuit model of the VCM.

The net deflection along F is

$$\delta = \sqrt{\delta_x^2 + \delta_y^2}. \tag{8}$$

Assuming small motions of the bobbin, thus, $\delta = D\theta$. Henceforth

$$k_\theta = \frac{M}{\theta} = \frac{4FD}{\delta/D} = \frac{48EI_w\left(D_x^2 + D_y^2\right)}{L^3\sqrt{(D_x/D)^2 + (D_x/D)^2}} \tag{9}$$

where D_x and D_y are, respectively, as shown in Fig. 4(b), the distances in the x- and y-directions between the bobbin center and each wire.

B. Modeling of Voice Coil Motors

The electromagnetic forces acting on the bobbin in the directions of focusing, tracking, and tilting are parameterized in this section. The actuators composed of sets of coils in the pickup are namely voice coil motors (VCMs), which are the electromagnetic dynamic balances of which, in pickup operation, as equivalently shown in Fig. 5, can be derived based on the Kirchhoff's law, yielding

$$\begin{aligned} V_{m(x,y,\theta)} &= R_m \cdot i_m + L_m \frac{di_m}{dt} + V_{mb} \\ &= R_m \cdot i_m + L_m \frac{di_m}{dt} + K_{mvs} \cdot \dot{q}_{(x,y,\theta)} \end{aligned} \tag{10}$$

where $V_{m(x,y,\theta)}$ are the independent VCM input voltages in three directions, V_{mb} is the back electromotive force (EMF), and $\{R_m, i_m, L_m$ and $K_{mvs}\}$ represent the resistance, current, inductance, and back EMF constant of the VCMs, respectively. With the electrical dynamics in (10) derived, the Fleming's left-hand rule [35] is then employed to derive the electromagnetic forces for actuation, which is

$$\begin{aligned} F_{(x,y,\theta)} &= n_m \cdot B_m \cdot l_m \cdot i_m \\ &= \left(\frac{n_m \cdot B_m \cdot l_m}{R_m}\right) \\ &\quad \times \left(V_{m(x,y,\theta)} - L_m \frac{di_m}{dt} - K_{mvs} \cdot \dot{q}_{(x,y,\theta)}\right) \end{aligned} \tag{11}$$

where n_m is the number of coil loops, B_m is the magnetic flux density within the air gap between the bobbin and magnets, and l_m is the total effective coil length for a single coil loop. Based

on the fact that the electrical dynamics of the conducted current are much faster than those mechanical ones in the directions of focusing, tracking, and tilting, the term $L_m(di_m)/(dt)$ in (11) can be neglected. Incorporating further the simplified $F_{(x,y,\theta)}$ in (11) into the system model in (5) arrives at a net system model with additional consideration of wire damping as

$$\mathbf{M}\ddot{\mathbf{q}} + \mathbf{C}_0\dot{\mathbf{q}} + \mathbf{K}_0\mathbf{q} + \mathbf{N} + \mathbf{G} = \bar{\mathbf{T}}_0\mathbf{V} \tag{12}$$

where $\mathbf{V}$ is of the form $\mathbf{V} = [V_x \quad V_y \quad V_\theta]^T$ which contains the input voltages into the VCMs in three DOFs of tracking, focusing, and tilting, respectively. The remaining two expressions in (12), $\mathbf{C}_0$, and $\bar{\mathbf{T}}_0$, are given as shown at the bottom of the page.

C. Modeling of Uncertainties and Disturbances

There often exist an uneven magnetic filed generated by magnets and manufacturing tolerances with respect to various crucial dimensions of the pickup structure, which are the factors, other than the movement of the bobbin, causing the mispasses of the electromagnetic forces on the mass center of the bobbin; as a result, this leads to a nonzero tilting. For later control design, the uncertainties due to the uneven magnetic field and manufacturing tolerance are formulated into the dynamical model in (12) as structured parametric uncertainties [36]. The formulation process is similar to that provided in [9], the details of which are omitted for the sake of simplicity. The formulation finally yields the system equations as

$$\mathbf{M}\ddot{\mathbf{q}} + \mathbf{C}\dot{\mathbf{q}} + \mathbf{K}\mathbf{q} + \mathbf{N} + \mathbf{G} + \tilde{\mathbf{D}} = \bar{\mathbf{T}}\mathbf{V} \tag{13}$$

where $\mathbf{C} = \mathbf{C}_0 + \mathbf{C}_\Delta, \mathbf{K} = \mathbf{K}_0 + \mathbf{K}_\Delta$, and $\bar{\mathbf{T}} = \bar{\mathbf{T}}_0 + \bar{\mathbf{T}}_\Delta$. $\mathbf{C}_\Delta, \mathbf{K}_\Delta$, and $\bar{\mathbf{T}}_\Delta$ are the modeled uncertainties associated with their nominal valuess $\mathbf{C}_0, \mathbf{K}_0$, and $\bar{\mathbf{T}}_0$, respectively. The detailed expressions of $\mathbf{C}_\Delta, \mathbf{K}_\Delta$, and $\bar{\mathbf{T}}_\Delta$ are provided in [9]. On the other hand, in (13), $\tilde{\mathbf{D}}$ is in fact $\tilde{\mathbf{D}} = [v_{d,x} \quad v_{d,y} \quad 0]^T$, where $v_{d,x}$ and $v_{d,x}$ are the disturbance resulting from the measured radial vibrations in the x- and y-directions, respectively. The measured radial vibrations are shown in time and frequency domains in Fig. 6, where it is seen that the practical radial vibratory disturbance consists of a primary harmonic of 1 μm at 7850 rpm, which is exactly the disk rotational frequency.

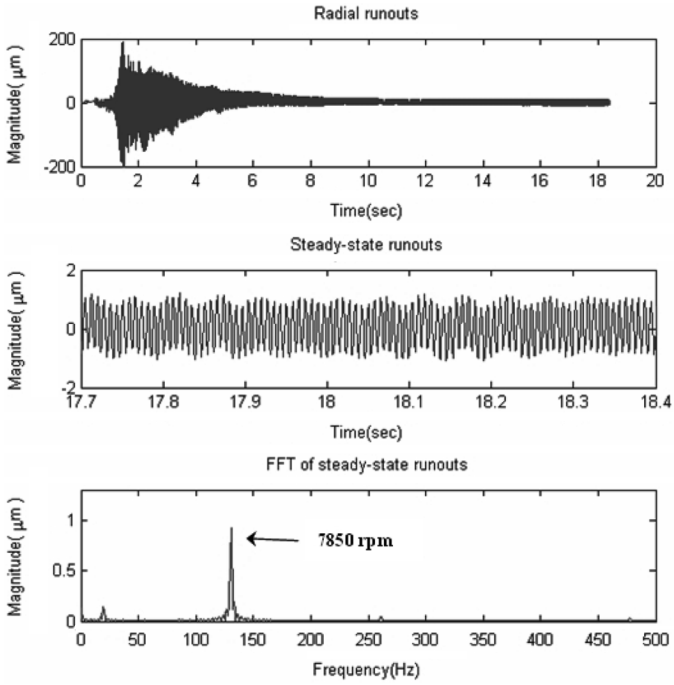

Fig. 6. Time trace and fast Fourier transform of measured runouts.

III. Design of the Sliding-Mode Controller

An SMC is synthesized here for precision positioning of the pickup actuator in three DOFs. This well-designed SMC is expected to accept the estimated states of $\mathbf{q}$ and $\dot{\mathbf{q}}$ from the high-gain observer and the sliding-mode observer designed later in this section and then to calculate required control efforts $\mathbf{V}$ to be fed to the optical pickup. Fig. 7 illustrates the system in a block diagram.

A. SMC

The design of the SMC starts with rewriting (13) as

$$\ddot{\mathbf{q}} = -\mathbf{M}^{-1}\mathbf{C}\dot{\mathbf{q}} - \mathbf{M}^{-1}\mathbf{K}\mathbf{q} - \mathbf{M}^{-1}\mathbf{D} + \mathbf{M}^{-1}\bar{\mathbf{T}}\mathbf{V} \tag{14}$$

$$\mathbf{C}_0 = \begin{bmatrix} C_x + \left(\frac{n_x B_x l_x}{R_x}\right) K_{mvs,x} & 0 & 0 \\ 0 & C_y + \left(\frac{n_y B_y l_y}{R_y}\right) K_{mvs,y} & 0 \\ 0 & 0 & C_\theta + \left(\frac{n_\theta B_\theta l_\theta}{R_\theta}\right) K_{mvs,\theta} \end{bmatrix}$$

$$\bar{\mathbf{T}}_0 = \begin{bmatrix} \cos\theta \cdot \frac{n_x B_x l_x}{R_x} & -\sin\theta \cdot \frac{n_y B_y l_y}{R_y} & 0 \\ \sin\theta \cdot \frac{n_x B_x l_x}{R_x} & \cos\theta \cdot \frac{n_y B_y l_y}{R_y} & 0 \\ 0 & 0 & \frac{n_\theta B_\theta l_\theta}{R_\theta} \end{bmatrix}.$$

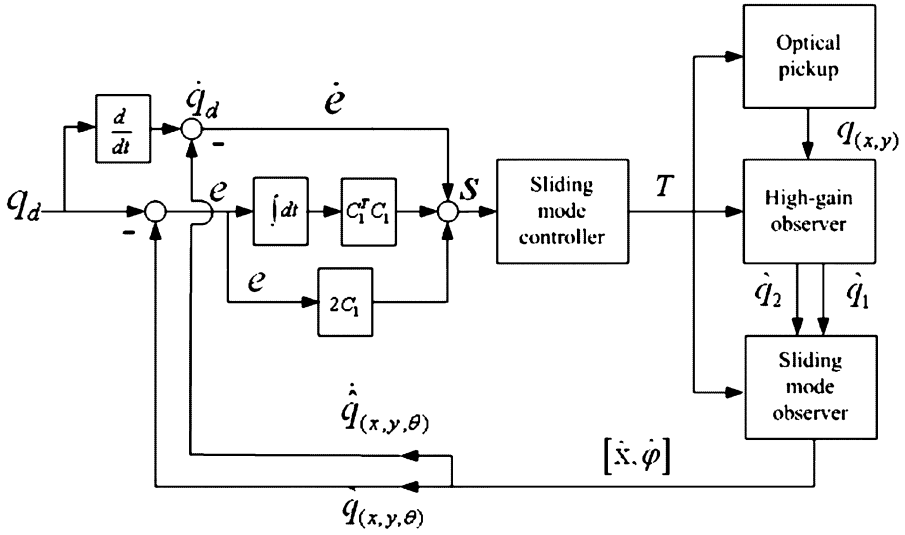

Fig. 7. Block diagram of the controlled system.

where $\mathbf{D} = (\mathbf{N} + \mathbf{G} + \tilde{\mathbf{D}})$. The error vector of the system is defined as

$$\mathbf{e} = \mathbf{q} - \mathbf{q_d} = \begin{bmatrix} X - X_d \\ Y - Y_d \\ \theta - \theta_d \end{bmatrix} \tag{15}$$

where $\mathbf{q_d} = [X_d \quad Y_d \quad \theta_d]^T$ are targeted focusing, tracking and tilting positions. Note that θ_d is set as zero to eliminate non-zero tilting. A switching vector function $S(e)$ containing the integrals of the positioning errors is next defined as

$$\mathbf{S(e)} = \left(\frac{d}{dt} + \mathbf{C}_1\right)^2 \left(\int_0^t \mathbf{e}dt\right) = \dot{\mathbf{e}} + \mathbf{2C}_1\mathbf{e} + \mathbf{C}_\mathbf{1}^T\mathbf{C}_1 \int_0^t \mathbf{e}dt \tag{16}$$

where $C_1 = \mathrm{diag}[C_{1,x}C_{1,y}C_{1,\theta}]$. Note that $\mathbf{C_1}$ is a matrix with positive diagonal elements to be determined. The determination of the elements in $\mathbf{C_1}$ decides relative convergence speeds among three DOFs. Taking time derivatives of $\mathbf{S(e)}$ in (16) and incorporating (14) and (15) leads to

$$\begin{aligned}\dot{\mathbf{S}} = (&-\mathbf{M}^{-1}\mathbf{C}\dot{\mathbf{q}} - \mathbf{M}^{-1}\mathbf{K}\mathbf{q} - \mathbf{M}^{-1}\mathbf{D} + \mathbf{M}^{-\mathbf{1}}\bar{\mathbf{T}}\mathbf{V}) \\ &-\ddot{\mathbf{q}}_\mathbf{d} + 2\mathbf{C_1}(\dot{\mathbf{q}} - \dot{\mathbf{q}}_\mathbf{d}) + C_1^T C_1(q - q_d).\end{aligned} \tag{17}$$

To find an appropriate control law, the reaching law of the states with proportional plus constant power rates in the form of

$$\dot{\mathbf{S}} = -P\mathbf{S} - \mathbf{Q}\,\mathrm{sgn}(\mathbf{S}) \tag{18}$$

is first set to be achieved. Note that $\mathbf{Q} = W \cdot \mathbf{diag}[|S_x|^\alpha \quad |S_y|^\alpha \quad |S_\theta|^\alpha]$ with S_x, S_y, S_θ being the components of the given sliding-mode matrix $\mathbf{S}$. Furthermore, P and W are positive weighting coefficients to be designed, while the choice of α also allows one to adjust the convergence speeds. By selecting appropriate values of P, W, and α in (18), the convergence of state trajectories to the switching surface can be guaranteed since the reaching law (18) directly leads to

$$\mathbf{S} \cdot \dot{\mathbf{S}} < \mathbf{0}. \tag{19}$$

To make possible the reaching law (18), the control efforts $\mathbf{V}$ in (17) can be designed as follows, based on theory of sliding-mode control:

$$\begin{aligned}\mathbf{V} &= [\boldsymbol{V}_\mathrm{x} \quad \boldsymbol{V}_\mathrm{y} \quad \boldsymbol{V}_\theta] \\ &= (\mathbf{M}^{-1}\bar{\mathbf{T}}_0)^{-1}\Big(\mathbf{M}^{-1}\mathbf{C}_0\dot{\mathbf{q}} + \mathbf{M}^{-1}\mathbf{K}_0\mathbf{q} \\ &\quad + \ddot{\mathbf{q}}_\mathbf{d} - \mathbf{C}_1\dot{\mathbf{q}} + \mathbf{C}_1\dot{\mathbf{q}}_d \\ &\quad - P\mathbf{S} - \mathbf{Q}\mathrm{sgn}(\mathbf{S}) + \mathbf{C}_1^\mathbf{T}\mathbf{C}_1\textstyle\int_0^\mathbf{t}(\mathbf{q} - \mathbf{q_d})dt\Big).\end{aligned} \tag{20}$$

By selecting large values of P and W for the control effort $\mathbf{V}$ in (20), one is not only able to reach the convergence in (19), but also retain the robustness against the uncertainties of $\mathbf{C}_\triangle, \mathbf{K}_\triangle$ and $\mathbf{T}_\triangle$ and the disturbance $\tilde{\mathbf{D}}$. Note that the necessary condition for reaching the robustness against the uncertainties and disturbance by the voltage input $\mathbf{V}$ in (20) is the satisfaction of the input matching condition [37]. This condition can, in fact, be easily proven satisfied, since the four-wire optical pickup is close to a typical spring-mass-damper system, as derived in (13), thanks to the smallness of nonlinearity $\mathbf{N}$ and gravity $\mathbf{G}$. Finally, in order to reduce the known chattering phenomenon near the switching surface, the function $\mathrm{sgn}(\mathbf{S})$ preproposed in (20) is replaced by a saturation function inside the predesignated boundary layer [13]. The saturation function is of the form

$$\mathrm{sat}(\mathbf{S}) = \left\{ \begin{array}{ll} \mathrm{sgn}(\mathbf{S}), & \mathrm{if}|\mathbf{S}| > \phi_s \\ \mathbf{S}/\phi_s, & \mathrm{if}|\mathbf{S}| \le \phi_s \end{array} \right\} \tag{21}$$

where ϕ_s is the boundary layer width of the switching surface.

B. High-Gain Observer

A high-gain observer is next synthesized and augmented into the controlled system in practice, as shown in Fig. 7, with the

aim to estimate the moving velocities of the bobbin in three DOFs of tracking, focusing, and tilting. The estimated velocities would be provided to the controller as the feedback signals in places of those digitally computed time derivatives from the measured displacements of the moving lens/bobbin. The replacements are motivated by the fact that the computed derivatives are often contaminated by the noises caused by sensor limitation and magnified by consequent digital discretization in practice.

The design process of the high-gain observer follows the procedure similar to that in [24] and [31], the details of which are not presented herein. This process finally yield an observer in the form of

$$\begin{aligned}\dot{\hat{\mathbf{q}}}_{\mathbf{1}} &= \hat{\mathbf{q}}_{\mathbf{2}} + \frac{1}{\varepsilon}\mathbf{H_p}(\mathbf{y} - \hat{\mathbf{q}}_{\mathbf{1}}) \\ \dot{\hat{\mathbf{q}}}_{\mathbf{2}} &= \frac{1}{\varepsilon^2}\mathbf{H_v}(\mathbf{y} - \hat{\mathbf{q}}_{\mathbf{1}})\end{aligned} \tag{22}$$

where $\hat{\mathbf{q}}_{\mathbf{1}}$ and $\hat{\mathbf{q}}_{\mathbf{2}}$ denote, respectively, the estimates of the actual displacements and velocities of the bobbin/lens, respectively. On the other hand, $\mathbf{H_p}$ and $\mathbf{H_v}$ are designated as the diagonal matrices with constant elements, i.e., $\mathbf{H_p} = \mathbf{diag}(h_{p,i})$ and $\mathbf{H_v} = \mathbf{diag}(h_{v,i})$, with the aim to achieve an estimation convergence for $\hat{\mathbf{q}}_{\mathbf{1}}$ and $\hat{\mathbf{q}}_{\mathbf{2}}$. Convergence of the estimation can be guaranteed, even against the uncertainties of $\mathbf{C}_\Delta, \mathbf{K}_\Delta$, and $\mathbf{T}_\Delta$, by choosing the values of $h_{p,i}$'s and $h_{v,i}$'s such that the spectra (roots) of the characteristic polynomials

$$p_i(\lambda) = \lambda^2 + h_{p,i}\lambda + h_{v,i}, \quad i = 1, 2 \tag{23}$$

are all in the left half plane. Finally, the value of ε in the observer in (22) is chosen as a small positive parameter, serving as a detuning parameter to adjust the convergence speed of the designed observer.

IV. Design of the Sliding-Mode Tilt Observer

A sliding-mode observer is synthesized in this section for estimating the tilting motion of the bobbin. A typical design procedure of a sliding-mode observer consists of two steps [24]. This starts with first arranging the dimensional controlled system (13) in state-space form as

$$\begin{aligned}\dot{\mathbf{x}} &= f_1(\mathbf{x}, \boldsymbol{\varphi}) \\ \dot{\boldsymbol{\varphi}} &= f_2(\mathbf{x}, \boldsymbol{\varphi})\end{aligned} \tag{24}$$

where

$$\begin{aligned}\mathbf{x} &\equiv [\,X \quad \dot{X} \quad Y \quad \dot{Y}\,]^T \\ &= [\,x_1 \quad x_2 \quad x_3 \quad x_4\,]^T \\ \boldsymbol{\varphi} &\equiv [\,\theta \quad \dot{\theta}\,]^T = [\,\varphi_1 \quad \varphi_2\,]^T \qquad (25) \\ f_1(\mathbf{x}, \boldsymbol{\varphi}) &= [\,x_2 \quad p_1 \quad x_4 \quad p_2\,]^T \\ f_2(\mathbf{x}, \boldsymbol{\varphi}) &= [\,\phi_2 \quad p_3\,]^T. \qquad (26)\end{aligned}$$

Note in (24) that $\mathbf{x}$ captures the measurable states, while $\boldsymbol{\varphi}$ does the states of bobbin tilting angle and velocity to be estimated by the observer. The sliding surface is next defined as the estimation errors between measurable states $\mathbf{x}$ and the estimates by the observer $\hat{\mathbf{x}}$, leading to

$$\mathbf{s} = [\,s_1 \quad s_2 \quad s_3 \quad s_4\,]^T \equiv \hat{\mathbf{x}} - \mathbf{x}. \tag{27}$$

The siding-mode observer is then designed to comprise

$$\dot{\hat{\mathbf{x}}} = \hat{f}_1(\hat{\mathbf{x}}, \hat{\boldsymbol{\varphi}}) - \mathbf{L}_x\mathbf{s} - \mathbf{K}_x\mathrm{sgn}(\mathbf{s}) \tag{28a}$$

$$\dot{\hat{\boldsymbol{\varphi}}} = \hat{f}_2(\hat{\mathbf{x}}, \hat{\boldsymbol{\varphi}}) - \mathbf{L}_\phi\mathbf{s} - \mathbf{K}_\phi\mathrm{sgn}(\mathbf{s}) \tag{28b}$$

where $\hat{f}$'s are the estimated model of the f's given in (24), $\mathbf{L}$'s and $\mathbf{K}$'s are gain matrices to be designed, and

$$\mathrm{sgn}(\mathbf{s}) = [\,\mathrm{sgn}(s_1) \quad \mathrm{sgn}(s_2) \quad \mathrm{sgn}(s_3) \quad \mathrm{sgn}(s_4)\,]^T. \tag{29}$$

The terms $\mathbf{L}_x\mathbf{s}$ and $\mathbf{L}_\phi\mathbf{s}$ in (28) provide linear error convergence outside the sliding surface, while $\mathbf{K}_x\mathrm{sgn}(\mathbf{s})$ and $\mathbf{K}_\phi\mathrm{sgn}(\mathbf{s})$ generate switching error-convergence efforts inside the sliding surface. Note that, from the term "$\mathbf{K}_\phi\mathrm{sgn}(\mathbf{s})$" in (28b) and (27), it is conceived that estimation of the nonmeasurable states $\boldsymbol{\varphi}$ are driven by the estimation error of the measurable states $(\hat{\mathbf{x}} - \mathbf{x})$. The dynamics of the error between the system and the estimates by the observer can be captured by subtracting (28) from (24), yielding

$$\dot{\tilde{\mathbf{x}}} = \Delta f_1(\hat{\mathbf{x}}, \hat{\boldsymbol{\varphi}}) - \mathbf{L}_x\mathbf{s} - \mathbf{K}_x\mathrm{sgn}(\mathbf{s}) \tag{30a}$$

$$\dot{\tilde{\boldsymbol{\varphi}}} = \Delta f_2(\hat{\mathbf{x}}, \hat{\boldsymbol{\varphi}}) - \mathbf{L}_\phi\mathbf{s} - \mathbf{K}_\phi\mathrm{sgn}(\mathbf{s}) \tag{30b}$$

where

$$\begin{aligned}\tilde{\mathbf{x}} &\equiv \hat{\mathbf{x}} - \mathbf{x} \\ \tilde{\boldsymbol{\varphi}} &\equiv \hat{\boldsymbol{\varphi}} - \boldsymbol{\varphi} \\ \Delta f_1 &\equiv \hat{f}_1 - f_1 \\ \Delta f_2 &\equiv \hat{f}_2 - f_2.\end{aligned}$$

Following the standard procedure of sliding-mode observer design, one can use the simple forms of $\mathbf{L}_x$ and $\mathbf{K}_x$ as

$$\mathbf{L}_x = \begin{bmatrix} l_x & 0 & 0 & 0 \\ 0 & l_x & 0 & 0 \\ 0 & 0 & l_x & 0 \\ 0 & 0 & 0 & l_x \end{bmatrix}$$

$$\mathbf{K}_x = \begin{bmatrix} \bar{k}_x & 0 & 0 & 0 \\ 0 & \bar{k}_x & 0 & 0 \\ 0 & 0 & \bar{k}_x & 0 \\ 0 & 0 & 0 & \bar{k}_x \end{bmatrix} \tag{31}$$

with large l_x and $\bar{k}_x$ to reach the convergence of $\tilde{\mathbf{x}} \to 0$. However, due to the complex nonlinearity involved in the term Δf_1 in (30a), which lays great difficulty in determining values of l_x and $\bar{k}_x$, the standard procedure of sliding-mode observer design cannot be employed herein to determine the observer gains of l_x and $\bar{k}_x$. To solve this problem, the error (30a)–(b) are simplified by only considering the first linear terms of Δf_1 and Δf_2, yielding the approximate linearized model of

$$\dot{\tilde{\mathbf{x}}} = \mathbf{F}_{11}\tilde{\mathbf{x}} + \mathbf{F}_{12}\tilde{\boldsymbol{\varphi}} - \mathbf{L}_x\mathbf{s} - \mathbf{K}_x\mathrm{sgn}(\mathbf{s}) \tag{32a}$$

$$\dot{\tilde{\boldsymbol{\varphi}}} = \mathbf{F}_{21}\tilde{\mathbf{x}} + \mathbf{F}_{22}\tilde{\boldsymbol{\varphi}} - \mathbf{L}_\phi\mathbf{s} - \mathbf{K}_\phi\mathrm{sgn}(\mathbf{s}) \tag{32b}$$

where

$$\mathbf{F}_{11}=\frac{\partial f_1}{\partial \mathbf{x}};\quad \mathbf{F}_{12}=\frac{\partial f_1}{\partial \boldsymbol{\varphi}};\quad \mathbf{F}_{21}=\frac{\partial f_2}{\partial \mathbf{x}};\quad \mathbf{F}_{22}=\frac{\partial f_2}{\partial \boldsymbol{\varphi}}. \tag{33}$$

The entries in the above $\{\mathbf{F}_{11},\mathbf{F}_{12},\mathbf{F}_{21},\mathbf{F}_{22}\}$ own particular structures due to the characteristics of the system state form in (24), which yield

$$\mathbf{F}_{11}=\begin{bmatrix}0 & 1 & 0 & 0\\ \bar{A}_{11} & \bar{A}_{14} & \bar{A}_{12} & \bar{A}_{15}\\ 0 & 0 & 0 & 1\\ \bar{A}_{21} & \bar{A}_{24} & \bar{A}_{22} & \bar{A}_{25}\end{bmatrix}$$

$$\mathbf{F}_{12}=\begin{bmatrix}0 & 0\\ \bar{A}_{13} & \bar{A}_{16}\\ 0 & 0\\ \bar{A}_{23} & \bar{A}_{26}\end{bmatrix} \tag{33a}$$

$$\mathbf{F}_{21}=\begin{bmatrix}0 & 0 & 0 & 0\\ \bar{A}_{31} & \bar{A}_{34} & \bar{A}_{32} & \bar{A}_{35}\end{bmatrix}$$

$$\mathbf{F}_{22}=\begin{bmatrix}0 & 1\\ \bar{A}_{33} & \bar{A}_{36}\end{bmatrix} \tag{33b}$$

where zero entries of $\mathbf{F}$'s in (33) result from the reduced-order state-space representation for the original system in (24). Note that the expressions of $\bar{A}$'s, the entries in the above $\mathbf{F}$'s, can be easily obtained by a basic standard computation procedure of linearization; therefore, they are omitted herein for the sake of concise presentation. Considering the linearized model in (32), the convergence condition for $\tilde{\mathbf{x}}\rightarrow 0$ based on the theory of the sliding-mode observer can be derived as

$$\mathbf{s}^T\dot{\mathbf{s}}=\tilde{\mathbf{x}}^T(\mathbf{F}_{11}\tilde{\mathbf{x}}+\mathbf{F}_{12}\tilde{\boldsymbol{\varphi}}-\mathbf{L}_x\tilde{\mathbf{x}}-\mathbf{K}_x\mathrm{sgn}(\tilde{\mathbf{x}}))<0. \tag{34}$$

From the structure of the above condition, one can set the gains of $\mathbf{L}_x$ sufficiently large to stabilize the eigenvalues of $(\mathbf{F}_{11}-\mathbf{L}_x)$, while also set the gains of $\mathbf{K}_x$ sufficiently large to let the term $\mathbf{K}_x\mathrm{sgn}(\tilde{\mathbf{x}})$ suppress the coupling term $\mathbf{F}_{12}\tilde{\boldsymbol{\varphi}}$. The corresponding lower limits of gains in $\mathbf{L}_x$ and $\mathbf{K}_x$ for satisfying condition (34) can be determined with known $\mathbf{F}_{11},\mathbf{F}_{12}$ and reasonable assumptions on the ranges of states during pickup operations. Since the process of deriving these limits is straightforward and tedious, they are not shown herein. Note that the gains of $\mathbf{L}_x$ and $\mathbf{K}_x$ are often and should be over-designed to achieve robustness for the observer. The next step is to determine the gain matrices associated with the unavailable states to estimate, i.e., $\mathbf{K}_\phi$ and $\mathbf{L}_\phi$. As $\tilde{\mathbf{x}}$ approaching zeros to satisfy condition (34), combination of (32a)–(32b) leads to

$$\dot{\tilde{\boldsymbol{\varphi}}}=\left(\mathbf{F}_{22}-\mathbf{K}_\phi\mathbf{K}_x^{-1}\mathbf{F}_{12}\right)\tilde{\boldsymbol{\varphi}}. \tag{35}$$

As long as the matrix $(\mathbf{F}_{22}-\mathbf{K}_\phi\mathbf{K}_x^{-1}\mathbf{F}_{12})$ in (35) is Hurwitz, the estimation error on the bobbin tilting and associated derivative in $\tilde{\boldsymbol{\varphi}}$ go to zero eventually. This can be accomplished by designing appropriate gains in $\mathbf{K}_\phi$. A special design procedure for determining $\mathbf{K}_\phi$ is proposed in the following to ensure convergence of $\tilde{\boldsymbol{\phi}}\rightarrow 0$ and further an easy control on the convergence rate. The design procedure for determining $\mathbf{K}_\phi$ starts with forcing $\mathbf{K}_\phi\mathbf{K}_x^{-1}$ to be in the form of

$$\mathbf{K}_\phi\mathbf{K}_x^{-1}=\begin{bmatrix}a_1 & 1\\ 0 & a_2\end{bmatrix}\begin{bmatrix}0 & N_{11} & 0 & N_{12}\\ 0 & N_{21} & 0 & N_{22}\end{bmatrix} \tag{36}$$

where N_{ij}'s satisfies

$$\begin{bmatrix}0 & N_{11} & 0 & N_{12}\\ 0 & N_{21} & 0 & N_{22}\end{bmatrix}\mathbf{F}_{12}=\mathbf{I}_{2\times 2} \tag{37}$$

and a's are to be assigned. Note that, with the special nature of $\mathbf{F}_{12}$—zero entries in the first and third rows, N_{ij}'s in (37) can be easily solved for given $\mathbf{F}_{12}$; then $\mathbf{K}_\phi$ can be determined based

TABLE I
GEOMETRIC AND MAGNETIC PARAMETERS OF THE VCM ACTUATOR

Description	Symbol	Value	Unit
Max voltage	$V_{m(\max)}$	5	volt
Max current	$i_{m(\max)}$	0.67	A
Resistance	R_x	7.5	Ohm
Resistance	R_y	7.5	Ohm
Resistance	R_θ	6.4	Ohm
Back EMF constant	$K_{ms,x}$	0.0416	volt/(m/sec)
Back EMF constant	$K_{ms,y}$	0.0416	volt/(m/sec)
Back EMF constant	$K_{ms,\theta}$	0.0357	volt/(m/sec)
Magnetic flux density	B_x	0.454	$\mathrm{Wb/m^2}$
Magnetic flux density	B_y	0.454	$\mathrm{Wb/m^2}$
Magnetic flux density	B_θ	0.454	$\mathrm{Wb/m^2}$
Effective length*	l_x	0.37	m
Effective length*	l_y	0.35	m
Effective length*	l_θ	0.1	m
No. of coil loops	n_x	32	loop
No. of coil loops	n_y	25	loop
No. of coil loops	n_θ	40	loop

* The effective lengths of the wires in focusing/tracking/tilting are total lengths of portions of the coil loops that induces actuating electro-magnetic forces, not the size of the coils in appearance.

TABLE II
CASES FOR CHOOSING WEIGHTINGS P AND W

Case No.	P	W	Positioning Errors in RMSEs		
			Tracking	Focusing	Tilting
1	5×10^3	10	0.802μm	0.576μm	1.30e-006°
2 (also for experiment)	5×10^4	10	0.434μm	0.461μm	7.91e-007°
3	5×10^5	10	0.467μm	0.462μm	3.50e-006°
4	5×10^4	10^3	0.447μm	0.447μm	8.14e-007°

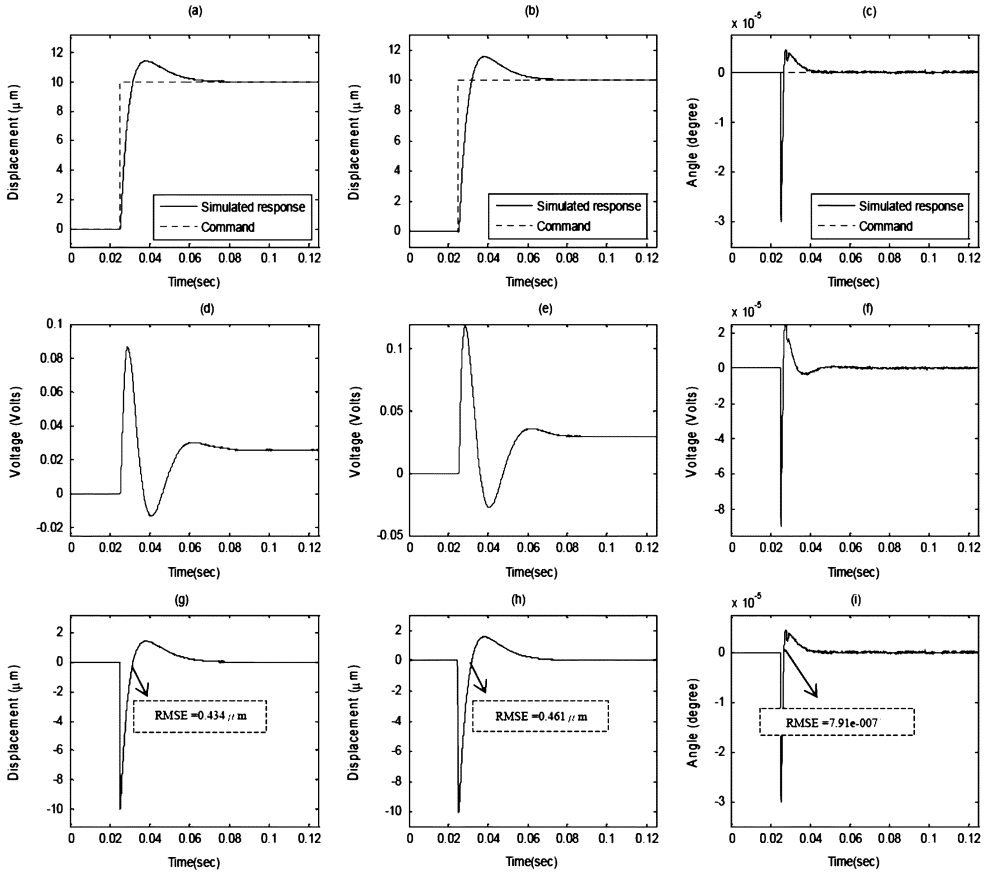

Fig. 8. Simulated step responses, control efforts, and errors of the pickup system controlled by the designed SMC in three directions with control parameters of Case 2 given in Table II. (a) Tracking position. (b) Focusing position. (c) Tilting angle. (d) Control effort. (e) Control effort. (f) Control effort. (g) Tracking position error. (h) Focusing position error. (i) Tilting angle error.

on (36) with predesigned $\mathbf{K}_x$. Incorporating (36) into system (35), one yields

$$\left(\mathbf{F}_{22}-\mathbf{K}_\phi\mathbf{K}_x^{-1}\mathbf{F}_{12}\right)=\begin{bmatrix}-a_1 & 0\\ \frac{\partial p_3}{\partial\phi_1} & \frac{\partial p_3}{\partial\phi_2}-a_2\end{bmatrix}. \tag{38}$$

Based on the particular structure of the matrix in (38), the eigenvalues of the system in (35) are $-a_1$ and $((\partial p_3)/(\partial\phi_2)-a_2)$. One can assign the speed of convergence for error estimation of the balancing ball $\tilde{\boldsymbol{\varphi}}$ by designating the values of a_1 and a_2 to enforce eigenvalues of $(\mathbf{F}_{22}-\mathbf{K}_\phi\mathbf{K}_x^{-1}\mathbf{F}_{12})$ to be the desired ones. With designated a_1 and a_2, $\mathbf{K}_\phi$ can be determined using (36) and (37) with predesigned $\mathbf{K}_x$.

It is pertinent to note that the proposed observer is forged based upon the linearized part of the subsystem due to the fact that the system possesses highly nonlinearity that makes the observer design based on the original nonlinear system almost impossible. With sufficiently large gains inside the matrices $\mathbf{K}_\phi$ and $\mathbf{L}_\phi$, even though the observer is designed from the linear part of the system, it still stands a fair chance to have a robust convergence of estimation.

V. Numerical Simulations

Numerical simulations are conducted here to find suitable controller parameters and observer gains. A practical three-axis pickup designed and manufactured by ITRI, as shown in Fig. 1, is used for the ensuing numerical simulations in this section and further experimental validation in the next section. All parameters of the considered three-axis four-wire-type optical pickup actuator are calibrated or obtained from documented properties. They are

$$\begin{aligned} m &= 2.87\times10^{-4}\ \text{kg}\\ L &= 12.5\times10^{-3}\ \text{m}\\ I_w &= 1.01\times10^{-17}\ \text{m}^4\\ E &= 1.1\times10^{11}\ \text{Pa}\\ r &= 4\times10^{-5}\ \text{m}\\ D_x &= 5.13\times10^{-3}\ \text{m}\\ D_y &= 1.225\times10^{-3}\ \text{m}\\ \Delta t &= 5\times10^{-4}\ \text{s}\\ I_{O\theta} &= 1.97\times10^{-9}\ \text{kg}\cdot\text{m}^2\\ I_x &= 2.38\times10^{-9}\ \text{kg}\cdot\text{m}\\ I_y &= 3.47\times10^{-9}\ \text{kg}\cdot\text{m} \end{aligned} \tag{39}$$

while the parameter values of the VCMs are given in Table I. Note that all of the physical meanings of the notations in (39) were previously given in Section II.

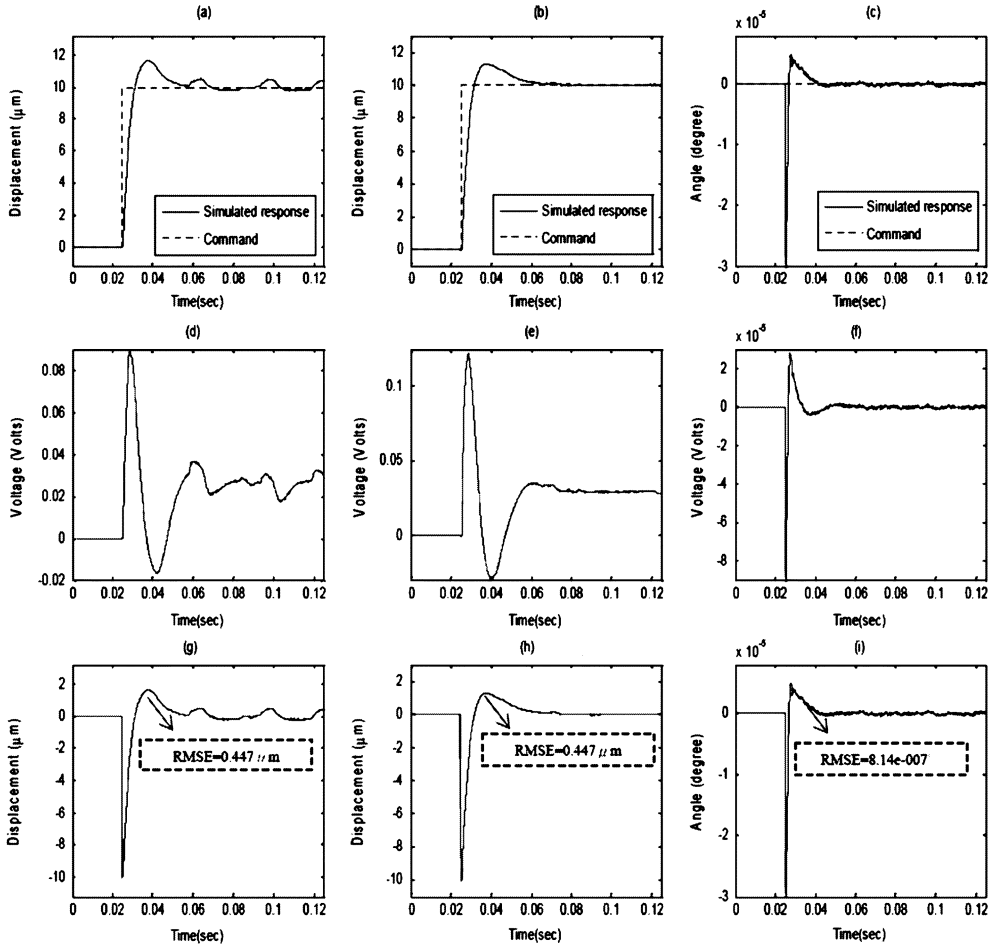

Fig. 9. Simulated step responses, control efforts, and errors of the pickup system controlled by the designed SMC in three directions with control parameters of Case 4 given in Table II. (a) Tracking. (b) Focusing. (c) Tilting. (d) Control effort. (e) Control effort. (f) Control effort. (g) Tracking error. (h) Focusing error. (i) Tilting error.

A. *Choosing Parameters of the SMC*

Numerical simulations on the controlled system are carried out here to choose appropriate parameter values for the SMC and the high-gain observer designed in Section III. The appropriateness can be ensured if the error convergence in (19) is reached in the presences of the disturbances due to radial burnouts, as specified by $\tilde{\mathbf{D}}$ in (13), and the parametric uncertainties, also in (13), which are prescribed as 5% of respective dimensions of the pickup bobbin. It can be obtained from the SMC design process proposed in Section III that the main control parameters affecting the controller performance are P, W, α and $\mathbf{C_1}$. Among these parameters, one can only consider P and W as the main parameters to be tuned for convergence and robustness, since the effects of α are only on the convergence which can also be tuned by P and W. On the other hand, $\mathbf{C_1}$ determines only the relative convergence speeds among the states. Therefore, in the following process of controller tuning, α is set to be unity to leave the job of convergence tuning to P and W, while $\mathbf{C_1}$ is designated as $\mathbf{C_1} = \mathrm{diag}[300\ 300\ 900]$ for reflecting desired relative convergence speeds among the states.

Four cases of varied P and W as listed in Table II are considered herein for simulations to obtain satisfactory controller performance with appropriately chosen values of P and W. The first, second, and third cases are integrally set to consider relative large, medium, and small levels of P and a fixed W, with the aim to find the most suitable value of P for better control convergence and robustness. With the desired trajectories in the x and y directions set to be step functions of 10 μm and the desired tilting in θ direction to be zero, simulations are conducted for the aforementioned four cases and the associated root mean squares of errors (RMSEs) of the bobbin positioning in three directions of tracking, focusing, and tiling are given in Table II. It can be seen from the RMSEs corresponding to Cases 1–3 in Table II that the case with the prechosen medium value of $P = 5 \times 10^4$ provides the best pickup actuation performance since it renders the smallest RMSE in all three directions. Fig. 8 presents the simulated time-domain responses for Case 2, where it is seen that the bobbin positionings in directions of focusing and tracking are achieved within 70 μs, while the positioning in the tilting direction to zero is accomplished in a shorter period of 30 μs. Of most importance is that the designed decoupling SMC is shown capable of containing an almost zero tilting angle to 7.91×10^{-7} deg as the bobbin is positioned to 10 μm in both focusing and tracking directions. In the next step, the simulations with the parameter values considered in Case 4 in

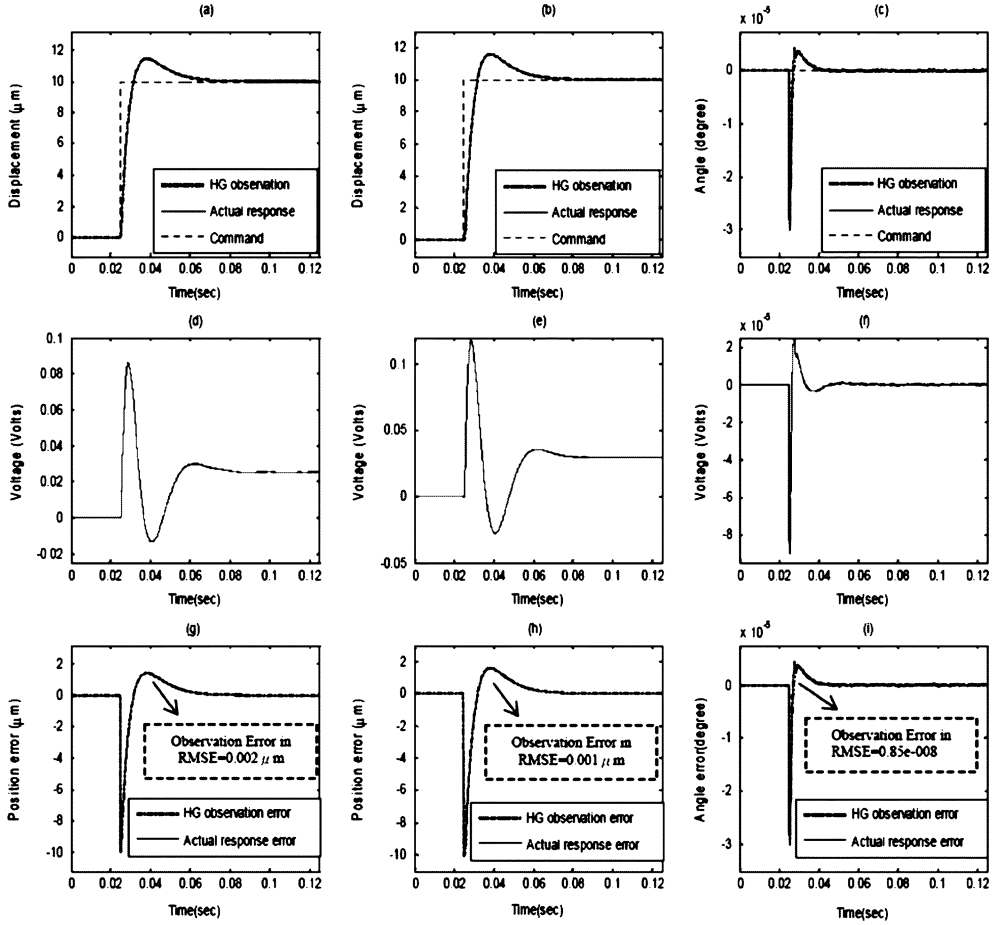

Fig. 10. Simulated step responses, control efforts, and errors of the pickup system controlled by the designed SMC assisted by the high-gain observer in three directions. The employed controller and observer parameters are those of Case 2 in Table III. (a) Tracking. (b) Focusing. (c) Tilting. (d) Control effort. (e) Control effort. (f) Control effort. (g) Tracking error. (h) Focusing error. (i) Tilting error.

Table II are conducted to find suitable value of W for a satisfactory controller performance. In Case 4, with P fixed to the pre-chosen medium value of 5×10^4, W is increased from the value of 10 in Cases 1–3 to 1000 for a chance to speed up the convergence near the sliding surface. The corresponding results are shown in Fig. 9. A general comparison between Figs. 8 and 9 renders that an increased W does not significantly shorten response time especially in the transient stage, while brings small levels of fluctuation due to the higher control gain of W near the sliding surface. The fluctuation is perceivable since W dictates level of the switching effort near the sliding surface. To avoid the fluctuation, the suitable value of W remains as the prechosen 10.

Efforts are next devoted to find suitable high-gain observer gains also based on simulations. In the first step, the values of parameters $h_{p,i}$'s and $h_{v,i}$'s to form the characteristic polynomial (23) are designated to lead to $\mathbf{H_p} = \mathbf{diag}[4\times10^3, 4\times10^3, 2\times10^4]$ and $\mathbf{H_v} = \mathbf{diag}[4\times10^6, 4\times10^6, 1\times10^8]$ with the aim to ensure robust stability of the observer. Second, the small parameter ε is first chosen as $\varepsilon = 0.005$ for a relative fast convergence on state velocity estimations. The resulted responses are plotted in Fig. 10, where the responses of the controlled system with the feedback velocities estimated from the high-gain observer are represented by dot-dashed curves, while those with those actual velocities are represented by solid curves for comparison. It is seen from the errors in Fig. 10(g)–(i) that the high-gain observer-based controller achieves precision positionings in the three DOFs of focusing, tracking, and tilting. Also, the RMSE values of the controlled system with the high-gain observer employed are close to those of actual responses in all three DOFs, indicating a satisfactory convergence in velocity estimation by the high-gain observer. ε is next detuned to a smaller value, $\varepsilon = 0.0005$, to aim for a better observer convergence. The corresponding RMSEs of the simulated response are given in the second row of Table III. It is seen from in Table III that all of the RMSEs for Case 2 are slightly smaller than their counterparts for Case 1. This indicates that a smaller $\varepsilon = 0.0005$ is a better

TABLE III
CASES FOR CHOOSING DETUNING PARAMETER ε

Case No.	P	Q	ε	Observation Errors in RMSEs		
				Tracking	Focusing	Tilting
1	5×10^4	10	0.005	0.01μm	0.013μm	0.88e-007°
2 (also for experiment)	5×10^4	10	0.0005	0.002μm	0.001μm	0.85e-007°

TABLE IV
CASES FOR CHOOSING OBSERVER GAINS $\bar{k}_x, a_1$, AND a_2

Case No.	$\bar{k}_x$	a_1 .	a_2	Positioning Errors in RMSEs			Observation Errors in RMSEs		
				Tracking	Focusing	Tilting	Tracking	Focusing	Tilting
1	50	10	10^2	0.453 μm	0.475 μm	2.945e-005°	0.001 μm	0.022 μm	2.543e-005°
2	1	10	10^2	0.453 μm	0.455 μm	4.072e-007°	0.001 μm	0.001 μm	0.0618e-007°
3 (also for experiment)	0.1	10	10^2	0.453 μm	0.455 μm	4.02157e-007°	0.001 μm	0.001 μm	0.01132e-007°
4	0.01	10	10^2	0.453 μm	0.455 μm	4.02157e-007°	0.001 μm	0.001 μm	0.00857e-007°
5	0.1	10^2	10^3	0.453 μm	0.455 μm	4.02159-007°	0.001 μm	0.001 μm	0.00959e-007°
6	0.1	0.1	1	0.453 μm	0.455 μm	2.826e-006°	0.001 μm	0.001 μm	2.543e-006°

choice than $\varepsilon = 0.005$. Note that the previous finding in fact reflects the theoretical core of the high-gain observer, that is, in each design of the observer, one ought to continuously detune the value of ε until the required computation load is bearable for the DSP module.

B. Choosing Parameters of the Sliding-Mode Observer

Further numerical simulations with varied gain values of the sliding-mode observer are carried out in this section to choose the appropriate ones to achieve fast observer error convergence on the tilting motion of the optical pickup. Based on the design procedure of the sliding-mode observer developed in the end of Section IV, the observer performance is dominated by the designed observer gains $l_x, \bar{k}_x, a_1$ and a_2. Among these gains, l_x and $\bar{k}_x$ are diagonal entries of the gain matrices as previously defined in (31) and they rule the convergence speed of the observation for available states, i.e., focusing and tracking motions, while a_1 and a_2, as previously defined in (36) and appearing in (38), dictate the convergence speed of unavailable states, i.e., tilting angle and the associated velocity of the moving bobbin, respectively. The process of determining all observer gains starts with l_x and $\bar{k}_x$. It is found based on theoretical ground and a number of simulations which are not shown for the sake of brevity that with varied l_x and $\bar{k}_x$ the convergence speed for measurable focusing and tracking motions can easily be tuned to desireds by simply increasing one of l_x and $\bar{k}_x$ to certain level, since both gains of l_x or $\bar{k}_x$ affects the convergence of available states simultaneously. Therefore, the following gain design process would only consider $\bar{k}_x$ as the tuning gain for available states with l_x fixed to 10, while a_1 and a_2 for unavailable states.

Six different combinations of $\bar{k}_x, a_1$, and a_2 listed in Table IV are considered to carry out simulations for the practical three-axis pickup designed and manufactured by ITRI, as shown in Fig. 1. The resulted performances of the designed controller and observer for the aforementioned six combinations are evaluated in terms of RMSEs for positioning and observation errors, also listed in respective cases in Table IV. Note that the positioning errors refers to the difference between the actual responses and the commands in three DOFs of the bobbin, while the positioning errors does the difference between the actual responses and the estimated counterparts provided by the predesigned sliding-mode observer. With a well-designed controller and observer, the actual responses ought to be settled at the commands with small RMSEs and close to the estimated counterparts provided by the sliding-mode observer at steady state. From the results of the first four cases in Table IV where only the gain of $\bar{k}_x$ is varied to choose its best value, it is seen that, as $\bar{k}_x$ is decreased from 50 of Case 1 to 0.1 of Case 3, the convergence is enhanced with evidence of RMSE for the tilting of actual responses deceased to around 4.02×10^{-7} deg, which is apparently a satisfied performance for tilt compensation. As further decreasing $\bar{k}_x$ to 0.01 of Case 4, the tilting RMSE remains around 4.02×10^{-7} deg, which indicates that, as determining $\bar{k}_x$, one can choose 0.1 or smaller for maximum performance. Fig. 11 depict the simulated system responses, control and observation errors for Case 3. It is seen from Fig. 11(g)–(i) that the precision focusing and tracking are well performed while, most importantly, the tilting of the pickup is totally annihilated with small observation errors within a short period of time, which is also clearly seen from the enlarged figure beside Fig. 11(c). It is also seen from Fig. 11(j)–(i) for observation errors that the sliding-mode observer has achieved a fast observation in tilting and satisfactory observation after the controller/observer scheme is activated around 0.3 s. With gain $\bar{k}_x$ determined, the second step is to determine gains of a_1 and a_2. Gains of a_1 and a_2 lower and higher than those in Cases 1–4 are considered in Cases 5 and 6, respectively, for investigating their effects on the observation convergence. Recall that a_1 affects the convergence speed of the bobbin tilt angle, while a_2 does the tilt velocity. Therefore, based on the theory of the sliding-mode observer, smaller gains of a_1 and a_2 as given in Case 6 stand a stronger risk losing observation convergence. A general comparison among Cases 3, 5, and 6 confirms the risk. As a_1 increased from 10 (Case 3) to 100 (Case 5) and a_2 from 100 (Case 3) to 1000 (Case 5), the observation convergence holds as evidenced from the unchanged resulted RMSEs given in Table IV. On the contrary, as a_1 decreased from 10 (Case 3) to 0.1 (Case 6) and a_2 from 100 (Case 3) to 1 (Case 6), the observation collapses as evidenced from a larger tilting RMSE

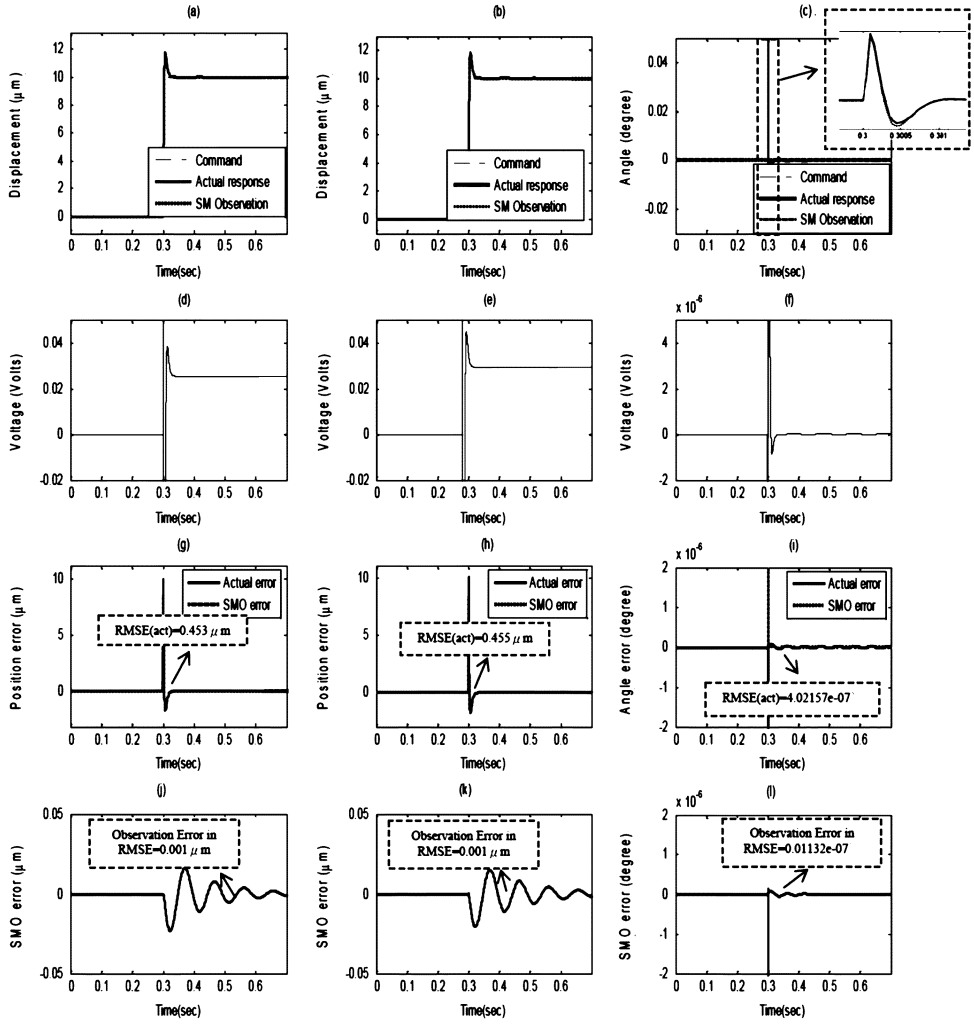

Fig. 11. Simulated step responses, control efforts, and errors of the pickup system controlled by the designed SMC assisted by the sliding mode observer in three directions. The employed controller and observer parameters are those of Case 3 in Table IV. (a) Tracking. (b) Focusing. (c) Tilting. (d) Control effort. (e) Control effort. (f) Control effort. (g) Tracking error. (h) Focusing error. (i) Tilting error. (j) Tracking observed error. (k) Focusing observed error. (l) Tilting observed error.

of the actual responses, 2.826×10^{-6}. Also seen from the results of Case 6 in this table is a large tilting RMSE of the observation error, 2.543×10^{-6}, indicating that the designed sliding-mode observer fail to estimate the tilting angle of the optical pickup within a required time frame. Fig. 12 depicts the simulated system responses, control, and observation errors for Case 6. It is seen from Fig. 12(i) and (l) that the observation errors appear unacceptably large at transient and steady states, which indicates the failure of the sliding-mode observer with overdecreased a_1 and a_2.

VI. Experimental Validation

Experiments are conducted to verify the expected effectiveness of the designed SMC and the accompanied sliding-mode tilt observer with the parameters and gains chosen in Section V. Fig. 13 illustrates the experimental setup employed, which consists of a laser displacement sensor (MTI 250), two optical fiber displacement sensors (MTI KD-300), and a three-axis pickup provided by the Industrial Technology and Research Institute (ITRI), Taiwan. The implementation of the previously designed controller/observer algorithms are accomplished by a DSP module (dSPACE1103) with sampling time interval of 100 μs. This DSP accepts the measurements of the bobbin motions from the laser and optical sensors, based on which calculations are conducted following the previously designed controller/observer algorithms to forge required output control efforts. The efforts are further amplified by a high-speed linear and bipolar amplifier (NF-HSA4051) before they are fed into the pickup for generating bobbin motions. The tracking motions of the bobbin (horizontal, along the X direction) in the pickup are measured directly by the laser displacement sensor, while the focusing motions (vertical, along the Y direction) are obtained by averaging two optical sensor signals. The averaging is conducted by the employed DSP module. The resolution of the laser displacement is up to 0.1 μm, while those of the optical sensors are around 0.3 μm. It should be also noted at this point that the laser and optical sensors used herein play integrally the role of the optical detection system employed in commercial pickups. As mentioned in the Introduction, several mature detection methods are available to provide the estimation on the bobbin motions. Fig. 2 illustrates some of commonly used systems and their working principles.

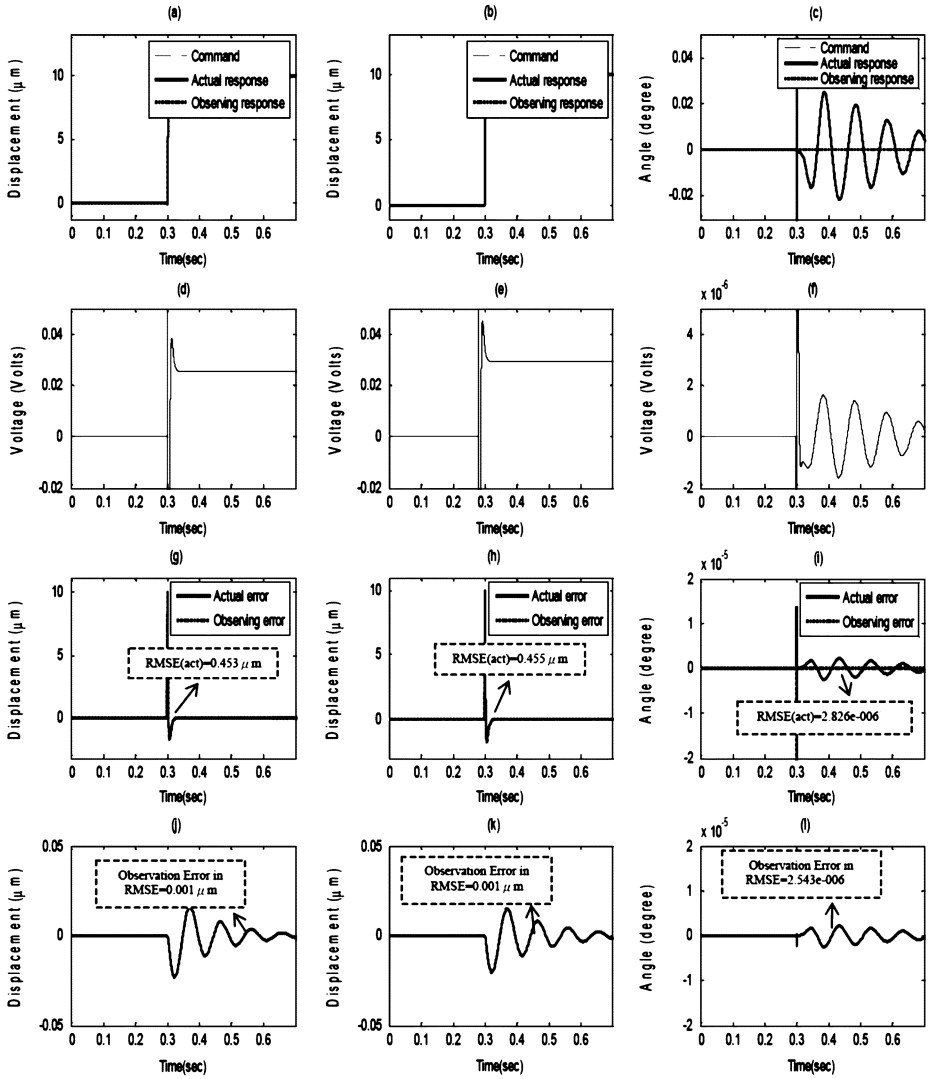

Fig. 12. Simulated step responses, control efforts, and errors of the pickup system controlled by the designed SMC assisted by the sliding mode observer in three directions. The employed controller and observer parameters are those of Case 6 in Table IV. (a) Tracking position. (b) Focusing position. (c) Tilting angle. (d) Control effort. (e) Control effort. (f) Control effort. (g) Positioning error. (h) Positioning error. (i) Angle error. (j) Error of observer. (k) Error of observer. (l) Error of observer.

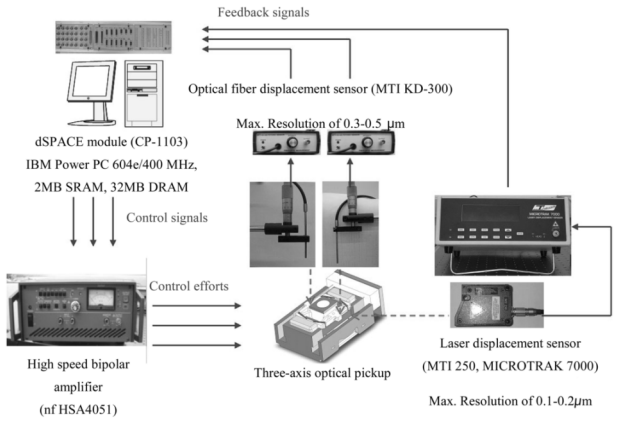

Fig. 13. Schematic diagram of the experimental setup.

Experiments with and without tilt compensation are carried out to verify the expected performance of the proposed controller and observers. The employed controller and observer gains were determined previously based on the simulations in Sections V-A and V-B, respectively. They corresponding cases are denoted as "for experiments" in Tables II–IV. Fig. 14 plots the experimental responses, control efforts, time histories of control, and observation errors with the theoretical counterparts for comparison. Also shown in Fig. 14(c), (i), and (l) are the tilt responses without the tilt compensation in dashed curves, compensation error, and observation error, respectively, for demonstrating the importance of tilt compensation. It is generically seen from Fig. 14(a)–(i) that the synthesized controller and observer are able to perform precision positionings simultaneously in the directions of tracking and focusing, and tilting compensation, rendering steady-state RMSEs of 0.115 μm, 0.258 μm and 0.0016°, respectively. Note that the RMSEs obtained herein for tracking and focusing are slightly below the resolutions of the used laser and optical sensors, respectively, thanks to the numerical integrations performed by the high-gain observer to reduce noises by the sensors and environment. Other than the posi-

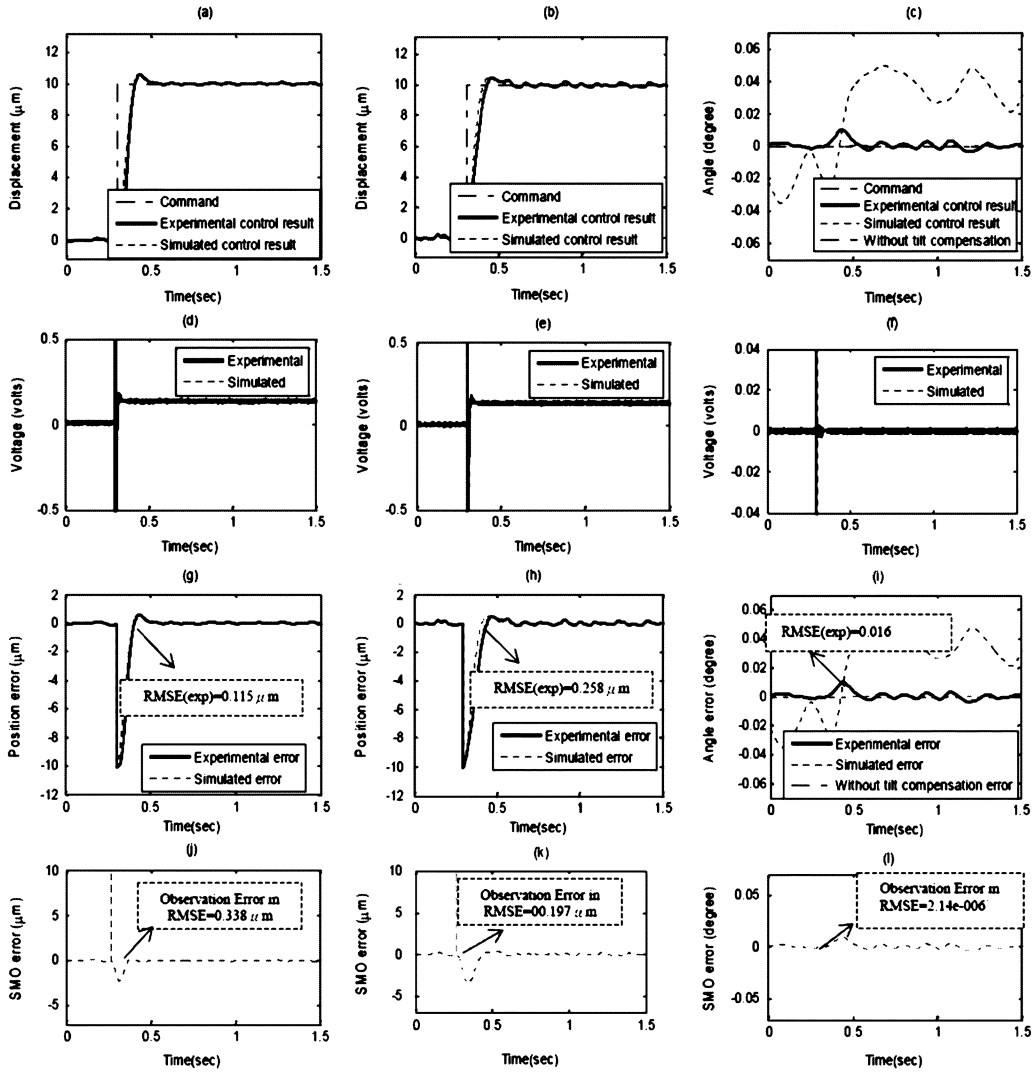

Fig. 14. Experimental and simulated step responses, control efforts, and errors of the pickup system controlled by the designed SMC assisted by the sliding mode tilt observer in three directions. (a) Tracking. (b) Focusing. (c) Tilting. (d) Control effort. (e) Control effort. (f) Control effort. (g) Tracking error. (h) Focusing error. (i) Tilt compensation error. (j) Tracking observation error. (k) Focusing observation error. (l) Tilting observation error.

tioning errors, small steady-state observation errors provided by the designed sliding-mode observer in three DOFs are also seen from Fig. 14(j)–(l), respectively. A general closeness is also present between the simulated curves and experimental counterparts. It should be noted from Fig. 14(c) and (i) that, without the tilt compensation implemented (simply switching off the control effort in the tilt direction), the pickup would not be able to contain the tilt at steady state. Finally, it should also be noted that the large fluctuations in the control efforts in Fig. 14(d) and (e) prior to the initiation of the step commands are due to the substantial estimation errors of the bobbin velocities induced by the high-gain observer. Based on theory of the high-gain observer convergence [31], the aforementioned observer estimation errors can easily be shown inevitable as the positioning errors are close to zeros—as before the step commands are initiated.

VII. Conclusion

This study is dedicated to perform sensorless tilt compensation and simultaneous precision positionings in directions of focusing and tracking for a three-axis optical pickup via design and experimental validation of an SMC equipped with a sliding-mode tilt observer. Based on the simulated and experimental results, the following conclusions are drawn.

1) Simulations and experimental studies have demonstrated the capability of the synthesized SMC and observer in performing simultaneous positioning of the bobbin in the pickup in the directions of focusing, tracking, and reducing tilting to acceptable, small levels without tilt sensor.
2) The levels of the tilting in the cases without tilt compensation activated are found to be substantially larger than those with the titling compensated by the designed SMC accompanied by a sliding-mode observer, showing the importance of employing a three-axis controller and the effectiveness of the accompanied controller/observer algorithm proposed in this study to suppress nonzero tilting.
3) The design and application of the sliding mode observer allows the SMC to perform tasks of decoupling and precision positioning of the moving bobbin without a tilt sensor

required, making possible an easy implementation of sensorless tilt compensation in commercial pickups.

ACKNOWLEDGMENT

The authors would like to thank the staff of the Industrial Technology and Research institute (ITRI), Taiwan, R.O.C., for their help with the experimental hardware and setup.

REFERENCES

[1] J. Zhang and L. Cai, "An autofocusing measurement system with a piezoelectric translator," *IEEE/ASME Trans. Mechatron.*, vol. 2, no. 3, pp. 213–216, Sep. 1997.

[2] K. C. Fan, C. Y. Lin, and L. H. Shyu, "Development of a low-cost focusing probe measurement," *Meas. Sci. Technol.*, vol. 11, pp. 1–7, 2000.

[3] K. C. Fan, C. Y. Lin, and L. H. Shyu, "Development of a low-cost autofocusing probe measurement," *Meas. Sci. Technol.*, vol. 12, pp. 2137–2146, 2001.

[4] M. Nagasato and I. Hoshino, "Development of two axis actuator with small tilt angles for one-piece optical head," *Jpn. J. Appl. Phys.*, vol. 35, pt. 1, pp. 392–397, 1996.

[5] I. H. Choi, S. N. Hong, M. S. Suh, D. H. Son, Y. L. Kim, K. W. Park, and J. Y. Kim, "3 axis actuator in slim optical pick-up for disc tilt compensation," in *Proc. Optical Storage Topical Meeting*, 2001, pp. 178–180.

[6] J. Y. Kang and M. G. Yoon, "Robust control of an active tilting actuator for high-density optical disk," in *Proc. Amer. Control Conf.*, 1998, vol. 2, pp. 861–865.

[7] Y. V. Martynov, B. H. W. Hendriks, F. Zijp, J. Aarts, J.-P. Baartman, V. G. Rosmalen, J. H. B. Schleipen, and H. V. Houten, "High numerical aperture optical recording: Active tilt or thin cover layer?," *Jpn. J. Appl. Phys. 2, Lett.*, vol. 38, no. 3B, pp. 1786–1792, 1999.

[8] S. Yamada, S. Nishiwaki, A. Nakamura, T. Ishida, and H. Yamaguchi, "Track center servo and radial tilt servo system for digital versatile rewritable disc (DVD-RAM)," *Jpn. J. Appl. Phys.*, vol. 39, pt. 1 2B, pp. 867–870, 2000.

[9] P. C.-P. Chao, J. S. Huang, and C. L. Lai, "Nonlinear dynamic analysis and actuation strategy for a three-dof four-wire type optical pickup," *Sens. Actuator A, Physical*, vol. 105, pp. 171–182, 2003.

[10] N. He, W. Jia, D. Yu, L. Huang, and M. Gong, "A novel type of 3 axis lens actuator with tilt compensation for high-density optical disc system," *Sens. Actuator A, Physical*, vol. 115, pp. 126–132, 2004.

[11] P. C.-P. Chao, C. L. Lai, and J. S. Huang, "Intelligent actuation strategy for a three-dof four-wire type optical pickup," *Sens. Actuators A, Physical*, vol. 117, pp. 28–40, 2004.

[12] P. C.-P. Chao and Y. S. Shen, "Design and experimental validation of an observer-based sliding-mode controller for a three axis four-wire type optical pickup," *Sens. Actuators A, Physical*, vol. 135, pp. 713–730, 2007.

[13] J. J. Slotine and W. Li, *Applied Nonlinear Control.*. Englewood Cliffs, NJ: Prentice-Hall, 1991.

[14] V. I. Utkin, *Sliding Modes and Their Applications in Variable Structure System*. Moscow, Russia: MIR, 1978.

[15] A. B. Marchant, *Optical Recording*. New York: Addison-Wesley, 1990.

[16] R. Katayama, S. Meguro, Y. Komatsu, and Y. Yamanaka, "Radial and tangential tilt detection for rewritable optical disks," *Jpn. J. Appl. Phys.*, vol. 40, no. 3B, pp. 1684–1693, 2001.

[17] K. Miyano and T. Nagara, "A new radial tilt detection method: Differential wobble phase detection," in *Proc. Optical Data Storage Conf.*, 2004, vol. 5380, pp. 189–196.

[18] F. Yamasaki, A. Arai, and H. Alkoh, "Radial tilt detection using push-pull signals," *Jpn. J. Appl. Phys.*, vol. 45, no. 2B, pp. 1158–1161, 2006.

[19] C. C. D. Wit and N. Fixot, "Robot control via robust estimated state feedback," *IEEE Trans. Autom. Control*, vol. 36, no. 12, pp. 1497–1501, Dec. 1991.

[20] C. C. D. Wit, N. Fixot, and K. J. Astrom, "Trajectory tracking in robot manipulators via nonlinear estimated state feedback," *IEEE Trans. Robot. Autom.*, vol. 8, no. 1, pp. 138–144, Feb. 1992.

[21] K. B. Park and T. Tsuji, "Continuous variable structure controller for robot manipulators using sliding mode observer," in *Proc. 5th Int. Workshop Advanced Motion Control*, 1998, pp. 506–511.

[22] C. Delepaut, G. Bastin, and M. Gevers, "Stabilization of nonlinear systems means of state estimate feedback," in *Proc. 28th Conf. Decision Control*, 1989, vol. 2, pp. 1042–1046.

[23] J. Hu, D. Zhu, Y. Li, and J. Gao, "Application of sliding observer to sensorless permanent magnet synchronous motor drive system.," in *IEEE Annu. Power Electron. Specialists Conf.*, 1994, vol. 1, pp. 532–536.

[24] J. J. E. Slotine, J. K. Hedrick, and E. A. Misawa, "On sliding observers for nonlinear systems," *J. Dynam. Syst., Meas., Control*, pp. 245–252, 1987.

[25] E. A. Misawa and J. K. Hedrik, "Nonlinear observer: A state-of-the art survey," *ASME J. Dynam. Syst. Meas.*, vol. 111, no. 3, pp. 344–352, 1979.

[26] I. Husain, S. Sodhi, and M. Ehsani, "A sliding mode observers based controller for switched reluctance motor drives," in *Conf. Rec. IEEE-IAS Annu. Meet.*, 1994, vol. 1, pp. 635–643.

[27] G. Besancon, "Further results on high gain observes for nonlinear systems," in *Proc 38th Conf. Decision Control*, 1999, vol. 3, pp. 2904–2909.

[28] A. Dabroom and H. K. Khalil, "Numerical differentiation using high-gain observers," in *Proc. 36th Conf. Decision Control*, 1997, vol. 5, pp. 4790–4795.

[29] J. A. Heredia and W. Yu, "A high-gain observer-based PD control for robot manipulator," in *Proc. Amer. Control Conf.*, 2000, vol. 4, pp. 2518–2522.

[30] A. Isidori, *Nonlinear Control Systems*, 3rd ed. Berlin, Germany: Springer-Verlag, 1995.

[31] H. K. Khalil, *Nonlinear Systems*, 3rd ed. Upper Saddle River, NJ: Prentice-Hall, 2002.

[32] S. Nicosia, A. Tornambe, and P. Valigi, "Experimental results in state estimation of industrial robots," in *Proc. 29th IEEE Conf. Decision Control*, 1990, vol. 1, pp. 360–365.

[33] E. S. Shin and K. W. Lee, "Robust output feedback control of robot manipulators using high-gain observer," in *Proc. Int. Conf. Control Appl.*, 1999, vol. 1, pp. 881–886.

[34] L. Meirovitch, *Analytical Methods in Vibrations*. London, U.K.: Macmillan, 1967.

[35] K. Milton, *Basic Electricity: Theory & Practice*. New York: McGraw-Hill, 1973.

[36] K. Zhou and J. C. Doyle, *Essentials of Robust Control*. Upper Saddle River, NJ: Prentice-Hall, 1998.

[37] H. Elmali and N. Olgac, "Robust output tracking control of nonlinear MIMO systems via sliding mode technique," *Automatica*, vol. 28, no. 1, pp. 145–151, 1992.

Paul C.-P. Chao received the B.S. degree from National Cheng-Kung University, Tainan, Taiwan, R.O.C., in 1989 and the M.S. and Ph.D. degrees from Michigan State University, Lansing, in 1993 and 1997, respectively.

After graduation, he worked for the CAE Department, Chrysler Corporation, Auburn Hill, MI, for two years. He is currently a Faculty Member of the Electrical and Control Engineering Department, National Chiao Tung University, Hsinchu, Taiwan. In recent years, his research interests focus on the electronics for optical systems; micro-mechatronics, control technology, micro- sensors, and actuators.

Prof. Chao was the recipient of the 1999 Arch T. Colwell Merit Best Paper Award from the Society of Automotive Engineering, the 2004 Long-Wen Tsai Best Paper Award from the National Society of Machine Theory and Mechanism, the 2005 Best Paper Award from the National Society of Engineers, Taiwan, the 2002/2003/2004 CYCU Innovative Research Award, the AUO Award in 2006, and the Acer Long-Term Second-Prize Award in 2007.

Chien-Yu Shen received the B.S.E. degree in civil engineering and the M.S. degree in mechanical engineering from Chung Yuan Christian University, Chung-Li, Taiwan, R.O.C., in 2002 and 2004, respectively. He is currently working toward the Ph.D. degree in mechanical engineering from Chung Yuan Christian University.

He specializes in mechanics of materials, mechanical dynamics, and system control theories include PID compensation, lead-lag compensation, fuzzy neural network control, and sliding-mode control theory. In order to practice novel optical data-reading systems, while pursuing his master's and doctoral degrees, he has inclined his efforts toward researching dynamic modeling of novel three-axis optical pickup head and design of controllers and observers for novel three-axis optical pickup heads. Furthermore, he also performed a cooperative plan of The Industrial Technology Research Institute in 2004, which is about development in auto-tuning algorithm of optical data-reading servo.